A Stabilized Finite Element Formulation Remedying Traction Oscillations in Cohesive Interface Elements

GOURAB GHOSH[1], CHANDRASEKHAR ANNAVARAPU[2] and RAVINDRA DUDDU[1]

ABSTRACT

The standard finite element implementation of intrinsic cohesive zone models (CZMs) based on the penalty method exhibits a distinct lack of numerical stability and/or convergence for stiff cohesive laws. This lack of stability is typically observed in the form of spurious oscillations in the normal and tangential tractions recovered at the cohesive interface. In this paper, we will present a robust, stabilized finite element formulation for CZMs that remedies traction oscillations, thus ensuring stability and convergence for any value of initial cohesive stiffness. A key advantage of the proposed formulation is that it generalizes the Nitsche's method for modeling cohesive fracture with a large initial cohesive stiffness, thus enabling the implementation of intrinsic and extrinsic CZMs in a unified and variationally consistent manner. We present several numerical examples to demonstrate the stability, convergence and accuracy of the proposed formulation in two-dimensions. First, we will verify the accuracy using simple patch tests considering uniaxial tension, compression and shear loadings. Second, we will demonstrate the lack of spurious traction oscillations at cohesive interfaces of rectangular beams loaded under shear and three-point bending. To demonstrate the stability issues related with the spurious traction oscillation, we consider both isotropic as well as anisotropic CZMs, wherein the normal and tangential cohesive stiffness values are different. Our numerical results for high stiffness cases clearly show that the proposed formulation yields a smooth oscillation-free traction profile and ensures stability, whereas the standard formulation suffers from instability and/or convergence issues.

---

[1]Department of Civil and Environmental Engineering, Vanderbilt University, Nashville, Tennessee.
[2]Atmospheric, Earth, and Energy Division, Lawrence Livermore National Laboratory, Livermore, California.

INTRODUCTION

Numerical simulation of fracture initiation and propagation in laminated composite materials is complex due to several plausible damage mechanisms, including fiber debonding, fiber breakage, and matrix cracking. Cohesive zone models (CZMs) are often used for modeling fracture propagation involving delamination or debonding at laminate interfaces. The advantage of CZMs is that they can be implemented within the finite element method by introducing zero-thickness interface elements along crack interfaces, whose constitutive behavior is defined by a traction-separation law or a cohesive law. In general, there are two classes of cohesive laws, namely intrinsic or initially elastic cohesive laws, and extrinsic or initially rigid cohesive laws. On the one hand, the extrinsic cohesive zone models may consistently describe fracture initiation at stiff cohesive interfaces, but are difficult to implement in a legacy finite element software (e.g., [1]). On the other hand, intrinsic CZMs are fairly straightforward to incorporate in a legacy finite element framework, but are plagued by numerical issues for stiff cohesive law. Specifically, the issue is that the finite element implementation can suffer from ill-conditioned discrete systems for "stiff" cohesive laws (i.e., cohesive stiffness is much greater than the value of bulk elastic modulus) or "anisotropic" cohesive laws (i.e., different normal and tangential cohesive stiffness), resulting in poor convergence and spurious oscillations in secondary variables such as interfacial tractions [2–4]. It bears emphasis that these issues can also arise with extrinsic CZMs during the analysis of stiff behavior under compressive loading or low-cycle fatigue loading, when unloaded and reloaded in the early stages of the softening regime of the traction-separation law [5].

In this work, we address the numerical issues associated with the finite element implementation of CZMs by generalizing the Nitsche's method to formulate a robust, stabilized formulation for treating stiff and/or anisotropic cohesive laws. The Nitsche's method [6] can be viewed as a variationally consistent penalty method, with the advantage that the discrete system of equations are better conditioned provided the stabilization parameters are chosen appropriately. As a result of the pioneering work of Hansbo [7], the method has become popular for a wide class of interface (contact) problems [8–10]. A more detailed account of the Nitsche's method and its application to various interface problems in computational mechanics can be found in the review article by [11]. While the Nitsche's method has been used in the context of contact problems before, to our knowledge, the extension to cohesive fracture problems is entirely new [12]. The rest of this paper is organized as follows: first, we will briefly introduce the model problem and present the generalized Nitsche formulation for cohesive laws; second, we will summarize the numerical implementation of the proposed formulation in the commercial software ABAQUS using user-defined subroutines; third, we will present numerical examples demonstrating the ability of the formulation to remedy spurious traction oscillations; and, finally, we conclude with a few closing remarks.

MODEL FORMULATION

In this section, we briefly present the details of the stabilized finite element formulation for cohesive fracture. We first present the strong form of the governing equations along with the brief description of the interface cohesive law. We next derive the weak form for the standard (penalty-like) and stabilized (Nitsche-based) using the standard Galerkin method of weighted residuals.

Strong Form

We define a domain $\Omega \subset \mathbb{R}^2$, which is partitioned into two non-overlapping bulk domains Ω^1 and Ω^2 (such that $\Omega = \Omega^1 \cup \Omega^2$) separated by a pre-defined cohesive interface Γ_* (Fig. 1). Both the bulk domains consist of a homogeneous isotropic linearly elastic material. Boundary conditions are defined on the parts of the domain boundary $\Gamma \equiv \partial\Omega$ excluding the interface Γ_*. The parts of the domain boundary where Dirichlet and Neumann conditions are prescribed are denoted as Γ_d and Γ_n, respectively and $\partial\Omega$=$\Gamma_d \cup \Gamma_n$ with $\Gamma_d \cap \Gamma_n$=$\emptyset$. The outward unit normal to the boundary $\partial\Omega$ is denoted by $\mathbf{n}_\mathrm{e}$ and unit normal vector associated with the interface boundary Γ_* is denoted by $\mathbf{n}$ and points from Ω^2 to Ω^1 (thus $\mathbf{n} = -\mathbf{n}^1 = \mathbf{n}^2$). The strong form of the linear elastostatic

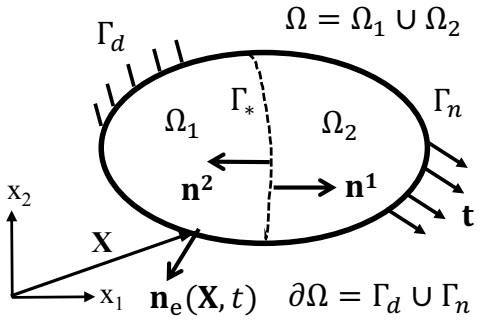

Figure 1: A schematic diagram of the domain for the linear elastostatic cohesive fracture problem

boundary value problem in absence of body force is [13]:

$$\boldsymbol{\nabla} \cdot \boldsymbol{\sigma} = \mathbf{0} \text{ in } \Omega, \tag{1}$$

$$\mathbf{u} = \mathbf{u}_d \text{ on } \Gamma_d, \tag{2}$$

$$\boldsymbol{\sigma} \cdot \mathbf{n}_e = \mathbf{t} \text{ on } \Gamma_n, \tag{3}$$

$$\mathbf{t}_c(\llbracket \mathbf{u} \rrbracket) = \boldsymbol{\sigma}^2 \cdot \mathbf{n}^2 = -\boldsymbol{\sigma}^1 \cdot \mathbf{n}^1 = f(\llbracket \mathbf{u} \rrbracket) \text{ on } \Gamma_*, \tag{4}$$

where $\mathbf{u}$ is the unknown displacement field vector, $\boldsymbol{\sigma}$ is the Cauchy stress tensor, $\mathbf{t}$ is the prescribed traction or stress vector on the Neumann boundary Γ_n, $\mathbf{u}_d$ is the prescribed displacement vector on the Dirichlet boundary Γ_d, and $\mathbf{t}_c$ is the traction on the crack interface. Because the traction is continuous across the interface, it can be related to the stress tensor on each domain as $\mathbf{t}_c = \boldsymbol{\sigma}^2 \cdot \mathbf{n}^2 = -\boldsymbol{\sigma}^1 \cdot \mathbf{n}^1$. The traction $\mathbf{t}_c$ can also be defined as a function of the interface separation $\boldsymbol{\delta}$= $[\![\mathbf{u}]\!] = \mathbf{u}^2 - \mathbf{u}^1$ based on an assumed cohesive law. Assuming small displacements, the Cauchy stress tensor can be defined as

$$\boldsymbol{\sigma} = \mathbf{D} : \boldsymbol{\epsilon}, \tag{5}$$

where $\mathbf{D}$ is the fourth order elasticity tensor and $\boldsymbol{\epsilon} = \frac{1}{2}(\nabla\mathbf{u} + (\nabla\mathbf{u})^T)$ is the small strain tensor defined as the symmetric gradient of the displacement vector.

Cohesive law

The intrinsic cohesive law defining a traction-separation relationship can be introduced by using the damage mechanics framework, which is detailed in [14, 15]. For simplicity, we consider a bilinear intrinsic traction separation law that has an initial (increasing) linear elastic portion followed by a (decreasing) linear softening response (see Fig. 2). To represent the mode I and mode II cohesive fracture behavior in two dimensions, we employ the normal and tangential coordinate system. Accordingly, the tangential (t_τ) and normal (t_n) components of the traction vector $\mathbf{t}_c$ are related to the normal (δ_n) and tangential (δ_τ) components of the interface separation as

$$\mathbf{t}_c\left([\![\mathbf{u}]\!]\right) = \begin{Bmatrix} t_\tau \\ t_n \end{Bmatrix} = (1 - d_s) \begin{bmatrix} \alpha_\tau^0 & 0 \\ 0 & \alpha_n^0 \end{bmatrix} \begin{Bmatrix} \delta_\tau \\ \delta_n \end{Bmatrix}, \tag{6}$$

where α_n^0 and α_τ^0 represent the initial cohesive stiffness in the normal and the tangential directions, respectively; δ_τ and δ_n represent the components of the interface separation vector in normal and tangential directions, respectively; d_s is the isotropic damage variable describing interface degradation under general mixed-mode loading as given by [16, 17]

$$d_s = \begin{cases} 0 & \text{if} \quad \delta_e < \delta_e^c \\ \dfrac{\delta_e^u(\delta_e - \delta_e^c)}{\delta_e(\delta_e^u - \delta_e^c)} & \text{if} \quad \delta_e^c < \delta_e < \delta_e^u \\ 1 & \text{if} \quad \delta_e^u < \delta_e \end{cases} \tag{7}$$

where $\delta_e = \sqrt{\delta_n^2 + \delta_\tau^2}$ is the equivalent separation, δ_e^c and δ_e^u are interface parameters corresponding to critical and ultimate separations, respectively, defined as [15, 17]

$$\frac{1}{\delta_e^c} = \sqrt{\left(\frac{\alpha_n^0 \cos I}{\sigma_{\max}}\right)^2 + \left(\frac{\alpha_\tau^0 \cos II}{\tau_{\max}}\right)^2} \tag{8}$$

$$\frac{1}{\delta_e^u} = \left(\frac{\alpha_n^0 \delta_e^c (\cos I)^2}{2\, G_{IC}}\right) + \left(\frac{\alpha_\tau^0 \delta_e^c (\cos II)^2}{2\, G_{IIC}}\right) \tag{9}$$

In the above equation, the direction cosines $\cos I = \delta_n/\delta_e$ and $\cos II = \delta_\tau/\delta_e$, $\sigma_{\max}$ and $\tau_{\max}$ are the pure mode I and mode II cohesive strengths, and G_{IC} and G_{IIC} are the pure mode I and mode II critical fracture energies. For monotonic loading, when the equivalent interface separation δ_e is less than the critical separation δ_e^c, there is no damage in the cohesive interface elements. After the critical separation is exceeded, damage starts to accumulate till the separation reaches the ultimate value δ_e^u, when the cohesive elements are completely damaged.

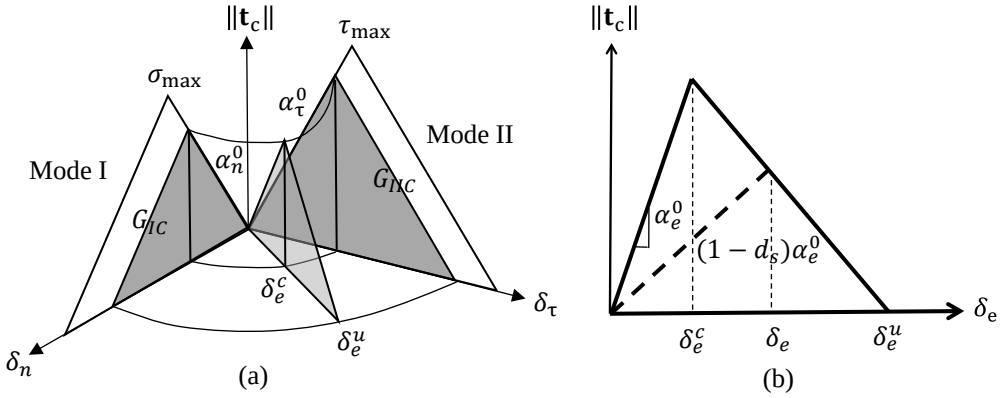

Figure 2: A schematic diagram of the mixed-mode bilinear cohesive law (redrawn from [18]): (a) the traction-separation relationship for any arbitrary mode-mix ratio is defined in terms of the pure mode I and mode II relationships; (b) the relationship between the static damage variable d_s and the equivalent separation

Weak Form

We follow the standard Galerkin finite element approximation to obtain the traditional weak form. The equilibrium equation Eq. (1) is weighted with a test function **w**, and after applying integration by parts we get the following expression:

$$\int_\Omega \nabla_s \mathbf{w} : \mathbf{D} : \nabla_s \mathbf{u}\, d\Omega - \int_{\Gamma_*} [\![\mathbf{w}]\!] \cdot \mathbf{t}_c\, d\Gamma = \int_{\Gamma_n} \mathbf{w} \cdot \mathbf{t}\, d\Gamma, \tag{10}$$

Upon substituting the cohesive traction-separation relations in normal and tangential directions,

we write the final expression for the standard weak form as

$$\int_{\Omega} \nabla_s \mathbf{w} : \mathbf{D} : \nabla_s \mathbf{u} \, d\Omega - \int_{\Gamma_*} (1 - d_s) \left([\![w_n]\!] \alpha_n^0 [\![u_n]\!] + [\![w_\tau]\!] \alpha_\tau^0 [\![u_\tau]\!] \right) \, d\Gamma = \int_{\Gamma_n} \delta \mathbf{u} \cdot \mathbf{t} \, d\Gamma. \quad (11)$$

When the initial cohesive stiffnesses α_n^0 and α_τ^0 are taken to be large (i.e., stiff intrinsic cohesive law), ill-conditioning may occur leading to instability and lack of convergence [2, 19].

To alleviate the ill-posedness of the weak form and ill-conditioning of the discretized system for stiff cohesive laws, we developed a Nitsche-method-based stabilized finite element formulation [12]. First, by pre-multiplying both the sides of Eq. (4) with a stabilization matrix **S** we obtain

$$\mathbf{S}\mathbf{t}_c([\![\mathbf{u}]\!]) = \mathbf{S}\boldsymbol{\sigma}^2 \cdot \mathbf{n}^2 = -\mathbf{S}\boldsymbol{\sigma}^1 \cdot \mathbf{n}^1 \ \text{ on } \ \Gamma_*. \quad (12)$$

Taking $\mathbf{n} = \mathbf{n}^2 = -\mathbf{n}^1$, we can write the above equation as

$$\mathbf{S}\mathbf{t}_c([\![\mathbf{u}]\!]) = \mathbf{S} \left\langle \boldsymbol{\sigma} \right\rangle_\gamma \cdot \mathbf{n} \ \text{ on } \ \Gamma_*, \quad (13)$$

where the weighted average of stress tensors on either side of the interface defined as

$$\left\langle \boldsymbol{\sigma} \right\rangle_\gamma = (\gamma^1 \boldsymbol{\sigma}^{\mathbf{1}} + \gamma^2 \boldsymbol{\sigma}^{\mathbf{2}}) \ \forall \ \gamma^1 + \gamma^2 = 1, \ \ \gamma^1 > 0, \ \ \gamma^2 > 0. \quad (14)$$

Next, by multiplying both the sides of Eq. (13) with the jump in the test function $[\![\mathbf{w}]\!]$ and integrating over the cohesive interface, we get

$$\int_{\Gamma_*} [\![\mathbf{w}]\!] \cdot \mathbf{S} \left\langle \boldsymbol{\sigma} \right\rangle_\gamma \cdot \mathbf{n} \, d\Gamma = \int_{\Gamma_*} [\![\mathbf{w}]\!] \cdot \mathbf{S}\mathbf{t}_c([\![\mathbf{u}]\!]) \, d\Gamma. \quad (15)$$

Finally, by adding the above Eq. (15) to the standard weak form in Eq. (10), we obtain the stabilized weak form for the exact same cohesive fracture problem as

$$\int_{\Omega} \nabla_s \mathbf{w} : \mathbf{D} : \nabla_s \mathbf{u} \, d\Omega - \int_{\Gamma_*} [\![\mathbf{w}]\!] \cdot (\mathbf{I} - \mathbf{S}) \left\langle \boldsymbol{\sigma} \right\rangle_\gamma \cdot \mathbf{n} \, d\Gamma - \int_{\Gamma_*} [\![\mathbf{w}]\!] \cdot \mathbf{S}\mathbf{t}_c([\![\mathbf{u}]\!]) \, d\Gamma = \int_{\Gamma} \delta \mathbf{u} \cdot \mathbf{t} \, d\Gamma \quad (16)$$

where **I** is the identity matrix, and $\mathbf{t}_c([\![\mathbf{u}]\!])$ denotes the interface cohesive law. In the above equation, the second term on the left hand side ensures consistency of the method and the third term on the left hand side ensures the stability of the method. Evidently, if we select the stabilization matrix **S** to be an identity matrix, the consistency term vanishes and the stabilized weak form in Eq. (16) reduces to the standard weak form represented by Eq. (10); whereas, if we choose **S=0**, the stability term vanishes and the stabilized weak form represents that corresponding to the perfectly bonded interface case. Proper choice of **S** (based on the criteria established in [8, 20, 21]) allows us to take extremely large values of α_n^0 and α_τ^0 without making the stabilized weak form variationally inconsistent or ill-posed.

NUMERICAL IMPLEMENTATION

We have implemented the proposed method in the commercial FE software ABAQUS through two user-defined subroutines: UELMAT to complete the bulk/continuum element computations, and UEL to complete the cohesive/interface element computations. The FORTRAN codes of these subroutines will soon be made available through our project website [22]. These subroutines are configured for bilinear quadrilateral plane strain elements using four-point Gauss integration scheme and four-noded linear cohesive elements using two-point Gauss integration scheme. Currently, we have the user element subroutines written for 2D plane strain and stress elements in Abaqus, but the stabilized method can be extended to 3D elements. An overview of the numerical implementation is provided below:

The algorithm for UELMAT subroutine is summarized as follows:

1. Compute the stiffness matrix and internal force vector for the bulk element
2. Assemble the stiffness matrix and the right hand side vector for the bulk element
3. Compute stress and shape function derivatives at interface Gauss integration points
4. Store computed stress and shape function derivatives in global modules

The algorithm for UEL subroutine is summarized as follows:

1. Compute the nodal cohesive separation
2. Calculate equivalent, equivalent critical and equivalent maximum separation
3. Compute static damage at interface element Gauss integration points
4. Calculate the stabilization matrix based on the stability criteria [8, 20, 21]
5. Compute the cohesive traction
6. Calculate the averaged stress using the information passed from the bulk element subroutine
7. Compute the weighted shape function derivative matrix using the information passed from the UELMAT subroutine through global modules
8. Compute the stabilized and consistency terms of the stiffness matrix
9. Partition and assemble consistency part of the stiffness matrix terms using dummy elements
10. Update the stiffness matrix of the user element
11. Compute the internal force of the cohesive element and update the right hand side vector of the user element

The presence of weighted average of stress and shape function derivatives across the interface implies that the computation of cohesive element tangent matrices and the residual vectors depends on the displacement shape functions associated with the nodes of the cohesive element, as well as those in the two neighboring bulk elements. In our numerical implementation, we calculate these quantities at the interface Gauss integration points in the UELMAT subroutine for the bulk elements, and then pass them to the UEL subroutine for the cohesive elements using global modules. These set of calculations are done separately from the standard loop over bulk Gauss integration points for assembling the bulk stiffness matrix and right hand side vector. The element tangent matrix is unsymmetric and the consistency part of the stiffness matrix has the dimension of 8×16, because the number of rows correspond to the 8 interfacial degrees of freedoms (DoFs) and the number of columns correspond to the 16 interfacial and adjacent bulk element DoFs. As the four-noded cohesive interface element has knowledge of only its 8 DoFs in the UEL subroutine, we can only assemble a stiffness matrix of size 8×8, which is main issue with implementing the stabilized formulation in Abaqus. However, we resolved this implementation issue by partitioning the 8×16 matrix into one 8×8 matrix and four 4×4 matrices and assembling them into the global stiffness matrix using "dummy" elements, as illustrated in Fig. 3.

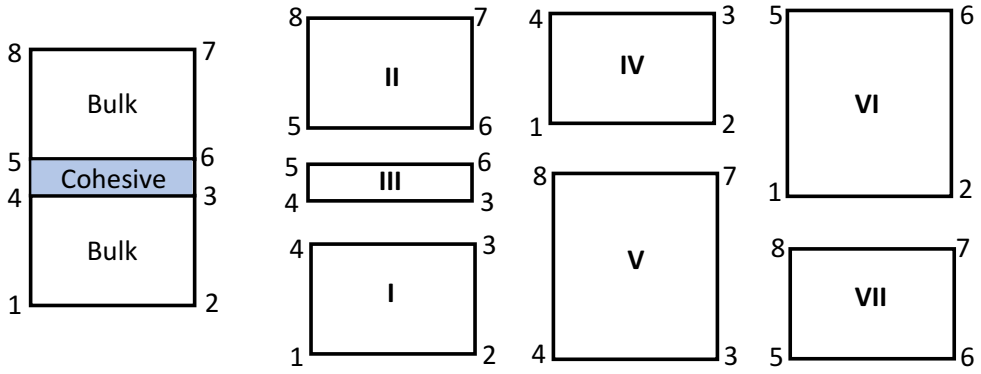

Figure 3: Assembly of the cohesive element matrix into the global tangent matrix in Abaqus. This requires the creation of four dummy elements (IV-VII) for each cohesive element (III) along with its two adjacent bulk elements (I and II).

NUMERICAL EXAMPLES

In this section, we first perform patch tests to assess the ability of the proposed stabilized finite element formulation to enforce perfect bonding at the cohesive interface before damage initiation, as usually defined in an extrinsic traction-separation law. Next, we simulate two benchmark tests for a rectangular plate loaded in shear and a rectangular notched beam with straight cohesive interfaces to illustrate the ability of the formulation to alleviate spurious traction oscillations. In all

Table I: THE ACCURACY OF THE STABILIZED METHOD TO ENFORCE PERFECTLY BONDED INTERFACE IN THE UNIAXIAL TENSION PATCH TEST. AS THE COHESIVE STIFFNESS TENDS TO INFINITY THE INTERFACE SEPARATION GOES TO MACHINE PRECISION.

Cohesive Stiffness (N/mm^3)	10^3	10^5	10^8	10^{15}	10^{20}	10^{100}
Displacement error (%) at node 6	96.61	22.17	2.84×10^{-2}	2.85×10^{-9}	1.39×10^{-14}	9.71×10^{-14}

these simulation studies, we assume linearly elastic isotropic bulk material behavior.

Patch Test for Verification

We conducted 2D patch tests by considering a computational domain defined by a unit square (1 mm $\times$ 1 mm) consisting of two bulk elements and one cohesive element as shown in Fig. 3. We first performed a uniaxial tension test by applying a vertical displacement $\Delta = 0.05$ mm at the upper two nodes (i.e., nodes 7 and 8), while constraining the bottom two nodes (i.e., nodes 1 and 2) using pinned and roller boundary conditions. The Young's modulus and Poisson's ratio of the isotropic elastic material in the bulk elements are assumed to be 10^5 N/mm^2 and 0.35, respectively. We calculated the percentage error between the computed vertical displacements at the middle nodes (i.e., nodes 3, 4, 5, 6) for different values of initial cohesive stiffness and the corresponding theoretical vertical displacement for infinite cohesive stiffness. The error values reported in Table I illustrate the accuracy of the proposed formulation in enforcing a perfectly bonded interface tends to machine epsilon (double precision) as the cohesive stiffness value is increased to large value. Even for an extremely high value of cohesive stiffness (i.e., 10^{100} N/mm^3) the stabilized formulation guarantees convergence; whereas, the standard formulation fails to converge beyond a moderately high value of cohesive stiffness (i.e., 10^{15} N/mm^3).

We also conducted uniaxial compression and simple shear tests using the same set up as before, with the only difference being that the direction of applied vertical displacement was reversed at the upper two nodes (i.e., nodes 7 and 8) for compression test, and horizontal displacements were applied at these nodes for shear test. We calculated the percentage error between the computed vertical and horizontal displacements at the middle nodes (i.e., nodes 3, 4, 5, 6) for different values of initial cohesive stiffness and the corresponding theoretical vertical displacement for infinite cohesive stiffness. The obtained error values are almost identical to those reported in Table I. We have also observed that for high values (e.g., 10^{20} N/mm^3 or 10^{30} N/mm^3) the standard formulation fails to converge, whereas the proposed formulation still yields an accurate solution. In summary, these patch tests clearly demonstrate that the stabilized formulation ensures convergence even for very large cohesive stiffness values, thus enabling us to enforce stiff cohesive laws without encountering any numerical instability.

Rectangular Plate Loaded in Shear

We considered a 16 mm $\times$ 5 mm rectangular plate with a vertical interface, as shown in Fig. 4. A vertical displacement of 1 mm is applied on the right edge of the plate, and both the horizontal and vertical displacements are constrained on the left edge. The Young's modulus and Poisson's ratio of the isotropic linearly elastic material in the bulk elements are assumed to be $E = 1$ N/mm^2 and $\nu = 0.2$, respectively, for illustration purposes. In Fig. 5, we plot the normal and tangential tractions at the cohesive interface for large values cohesive stiffness ($\alpha_n^0 = \alpha_\tau^0 = 10^{14}$ N/mm^3) obtained from the standard and stabilized formulations. Clearly, the traction profiles obtained from the stabilized formulation are free of any spurious oscillations, unlike the standard formulation. We note that the standard formulation fails to converge for extremely large values of cohesive stiffness (e.g., $\alpha_n^0 = \alpha_\tau^0 = 10^{25}$ N/mm^3), showing the lack of robustness. In contrast, the stabilized formulation guarantees convergence and stability for any value of cohesive stiffness. Fig. 6 shows the normal and tangential traction obtained from the standard and the proposed formulation for the anisotropic cohesive zone model ($\alpha_n^0 = 10^{14}$ N/mm^3 and $\alpha_\tau^0 = 10^{13}$ N/mm^3). Clearly, the standard formulation yields oscillations in normal and tangential traction profiles; whereas the stabilized formulation yields an oscillation-free traction profile, illustrating its stability.

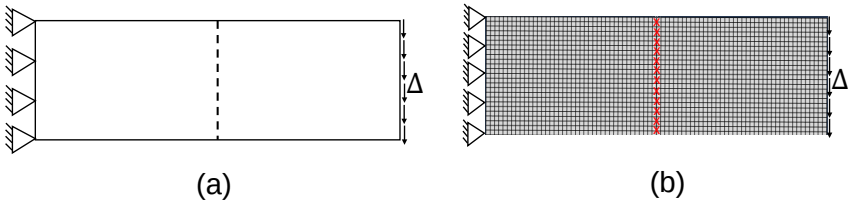

Figure 4: Rectangular plate loaded in shear: (a) schematic diagram; (b) finite element mesh.

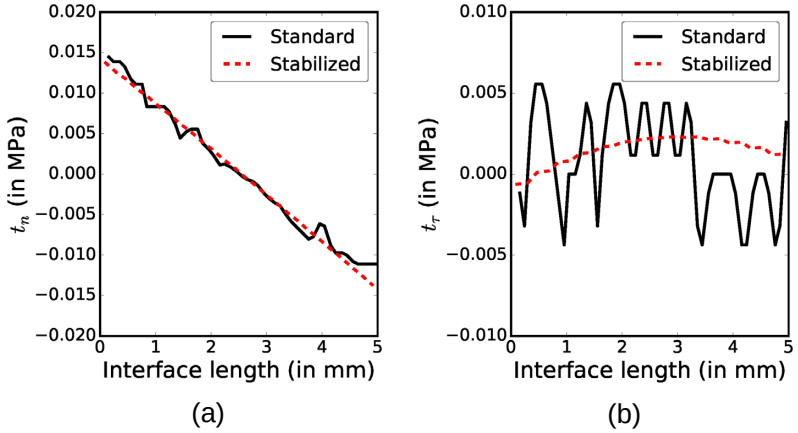

Figure 5: Simulation results for the rectangular plate in shear obtained from the standard and stabilized formulations for an isotropic cohesive zone model: (a) Normal and (b) tangential traction profile for $\alpha_n^0 = \alpha_\tau^0 = 10^{14}$ N/mm^3

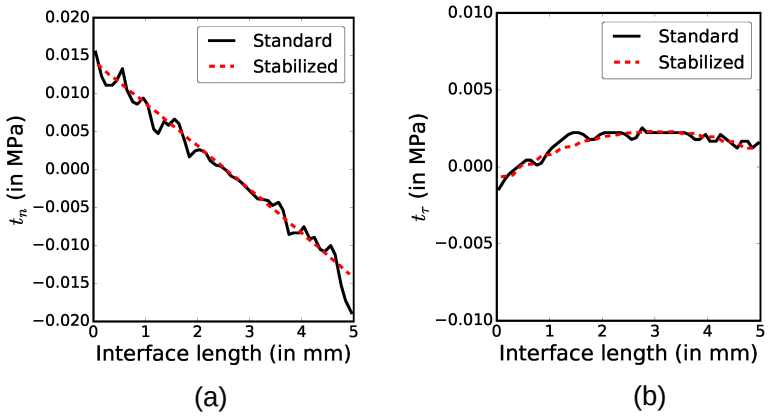

Figure 6: Simulation results for the rectangular plate in shear obtained from the standard and stabilized formulations for an anisotropic cohesive zone model: (a) Normal and (b) tangential traction profile for α_n^0= 10^{14} N/mm^3 and α_τ^0= 10^{13} N/mm^3

Rectangular Notched Beam

We considered a 450 mm $\times$ 100 mm rectangular beam with a vertical interface, as shown in Fig. 7. A vertical displacement of 10 mm is applied at the midpoint of the top edge of the beam, and the bottom two corner nodes are constrained using pinned and roller boundary conditions. The Young's modulus and Poisson's ratio of the isotropic linearly elastic material in the bulk elements are assumed to be $E = 2 \times 10^4$ N/mm^2 and $\nu = 0.2$, respectively. In Fig. 8, we plot the normal and tangential tractions at the cohesive interface for cohesive stiffness values of ($\alpha_n^0 = \alpha_\tau^0 = 10^8$ N/mm^3) obtained from the standard and stabilized formulations. We note that even for moderately large values of cohesive stiffness (i.e., 3–4 orders of magnitude larger than Young's modulus) the standard formulation yields an oscillations in traction profile at the ends of the cohesive interface, illustrating the instability. Clearly, the traction profiles obtained from the stabilized formulation are free of any spurious oscillations, unlike the standard formulation.

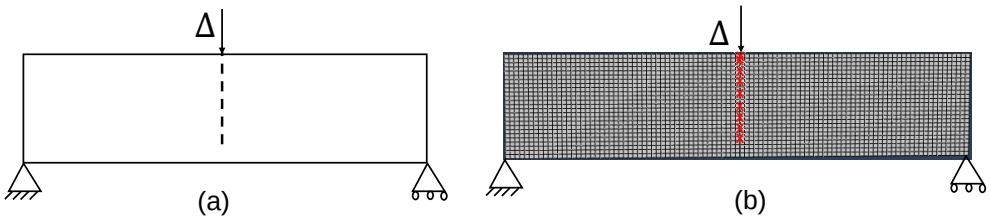

Figure 7: Rectangular notched beam: (a) schematic diagram; (b) finite element mesh.

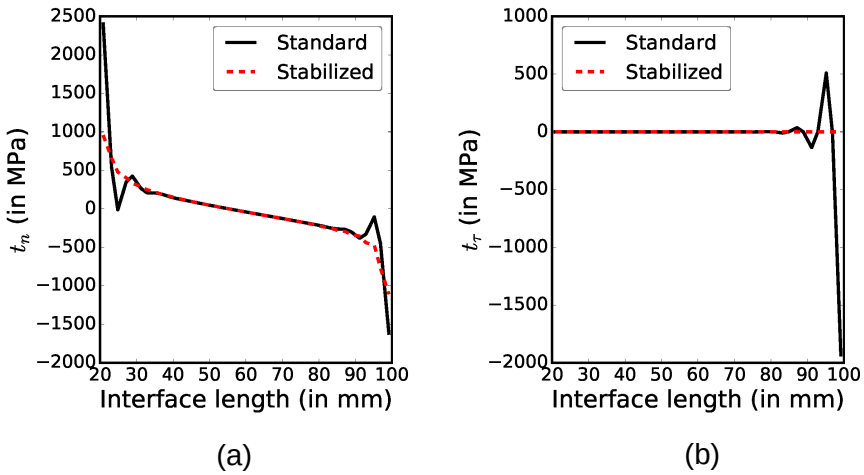

Figure 8: Simulation results for the notched beam obtained from the standard and stabilized formulations for an isotropic cohesive zone model: (a) Normal and (b) tangential traction profile for $\alpha_n^0 = \alpha_\tau^0 = 10^8$ N/mm^3

Conclusion

In this work, we illustrated the ability of the stabilized formulation for cohesive zone models, originally proposed in [12], for remedying traction oscillation in interface elements described by stiff cohesive laws. The proposed formulation generalizes the Nitsche method for cohesive fracture problems and allows us to use extremely large values of initial stiffness, thus providing a unified way to treat intrinsic and extrinsic cohesive zone models in a variationally consistent and stable manner. We performed numerical simulation studies that demonstrate the superior convergence behavior of the proposed formulation over the standard formulation based on the standard penalty method. The simulation studies also highlighted the lack of robustness and numerical instability issues associated with the traditional formulation and the efficacy of the proposed formulation in eliminating them. Our future work is focused on developing user subroutines for 3-D fracture propagation in composites subjected to monotonic and cyclic loading, including high-cycle fatigue delamination.

Acknowledgements

We gratefully acknowledge the funding from our sponsors: GG and RD were supported by the Office of Naval Research – award #N0014-17-12040 (Program Officer: Mr. William Nickerson).

References

[1] V.P. Nguyen. Discontinuous Galerkin/extrinsic cohesive zone modeling: Implementation caveats and applications in computational fracture mechanics. *Engineering Fracture Mechanics*, 128:37–68, 2014.

[2] A. Simone. Partition of unity-based discontinuous elements for interface phenomena: computational issues. *International Journal for Numerical Methods in Biomedical Engineering*, 20(6):465–478, 2004.

[3] N. Blal, L. Daridon, Y. Monerie, and S. Pagano. Artificial compliance inherent to the intrinsic cohesive zone models: criteria and application to planar meshes. *International Journal of Fracture*, 178(1-2):71–83, 2012.

[4] E. Svenning. A weak penalty formulation remedying traction oscillations in interface elements. *Computer Methods in Applied Mechanics and Engineering*, 310:460–474, 2016.

[5] R. Radovitzky, A. Seagraves, M. Tupek, and L. Noels. A scalable 3D fracture and fragmentation algorithm based on a hybrid, discontinuous Galerkin, cohesive element method. *Computer Methods in Applied Mechanics and Engineering*, 200(1):326–344, 2011.

[6] J. Nitsche. Über ein Variationsprinzip zur Lösung von Dirichlet-Problemen bei Verwendung von Teilräumen, die keinen Randbedingungen unterworfen sind. In *Abhandlungen aus dem mathematischen Seminar der Universität Hamburg*, volume 36, pages 9–15. Springer, 1971.

[7] A. Hansbo and P. Hansbo. A finite element method for the simulation of strong and weak discontinuities in solid mechanics. *Computer Methods in Applied Mechanics and Engineering*, 193(33-35):3523–3540, 2004.

[8] C. Annavarapu, M. Hautefeuille, and J.E. Dolbow. A robust Nitsche's formulation for interface problems. *Computer Methods in Applied Mechanics and Engineering*, 225:44–54, 2012.

[9] C. Annavarapu, M. Hautefeuille, and J.E. Dolbow. A Nitsche stabilized finite element method for frictional sliding on embedded interfaces. Part I: single interface. *Computer Methods in Applied Mechanics and Engineering*, 268:417–436, 2014.

[10] C. Annavarapu, R.R. Settgast, S.M. Johnson, P. Fu, and E.B. Herbold. A weighted Nitsche stabilized method for small-sliding contact on frictional surfaces. *Computer Methods in Applied Mechanics and Engineering*, 283:763–781, 2015.

[11] P. Hansbo. Nitsche's method for interface problems in computational mechanics. *GAMM-Mitteilungen*, 28(2):183–206, 2005.

[12] G. Ghosh, C. Annavarapu, S. Jiménez, and R. Duddu. A stabilized finite element method for modeling mixed-mode delamination of composites. In *Proceedings of the American Society for Composites: Thirty-Second Technical Conference, Purdue University, West Lafayette, Indiana, October 23–25*, pages 1–16, 2017.

[13] J. Mergheim, E. Kuhl, and P. Steinmann. A finite element method for the computational modelling of cohesive cracks. *International Journal for Numerical Methods in Engineering*, 63(2):276–289, 2005.

[14] X. Liu, R. Duddu, and H. Waisman. Discrete damage zone model for fracture initiation and propagation. *Engineering Fracture Mechanics*, 92:1–18, 2012.

[15] S. Jiménez and R. Duddu. On the parametric sensitivity of cohesive zone models for high-cycle fatigue delamination of composites. *International Journal of Solids and Structures*, 82:111–124, 2016.

[16] G. Alfano and M.A. Crisfield. Finite element interface models for the delamination analysis of laminated composites: mechanical and computational issues. *International Journal for Numerical Methods in Engineering*, 50(7):1701–1736, 2001.

[17] W.G. Jiang, S.R. Hallett, B.G. Green, and M.R. Wisnom. A concise interface constitutive law for analysis of delamination and splitting in composite materials and its application to scaled notched tensile specimens. *International Journal for Numerical Methods in Engineering*, 69(9):1982–1995, 2007.

[18] L.F. Kawashita and S.R. Hallett. A crack tip tracking algorithm for cohesive interface element analysis of fatigue delamination propagation in composite materials. *International Journal of Solids and Structures*, 49(21):2898 – 2913, 2012.

[19] J.C.J. Schellekens and R. De Borst. On the numerical integration of interface elements. *International Journal for Numerical Methods in Engineering*, 36(1):43–66, 1993.

[20] C. Annavarapu, M. Hautefeuille, and J.E. Dolbow. Stable imposition of stiff constraints in explicit dynamics for embedded finite element methods. *International Journal for Numerical Methods in Engineering*, 92(2):206–228, 2012.

[21] A. Embar, J. Dolbow, and I. Harari. Imposing Dirichlet boundary conditions with Nitsche's method and spline-based finite elements. *International Journal for Numerical Methods in Engineering*, 83(7):877–898, 2010.

[22] G. Ghosh, S. Jiménez, and R. Duddu. Abaqus User Element Subroutines for the stabilized cohesive zone formulation. `https://my.vanderbilt.edu/cpml/research/onr-n0014-17-12040/`. Accessed: 2018-06-30.